JEE Journal of Ecological Engineering

Journal of Ecological Engineering, 2026, 27(10), 226–243
https://doi.org/10.12911/22998993/xxxxx
ISSN 2299–8993, License CC-BY 4.0

Received: 2026.06.18
Accepted: 2026.07.24
Published: 2026.09.01

Manganese(II) removal from aqueous solutions by adsorption on drinking water treatment sludge

Carolina de Camargo Barbosa[1], Lucila Adriani de Almeida Coral[2], Flavio Francisco Ivashita[3], Paulo Rodrigo Stival Bittencourt[4], Marcela Fernandes Silva[1], Cláudia Telles Benatti[1*]

[1] State University of Maringá, Postgraduate Programme in Urban Engineering, Maringá-PR, Brazil
[2] Federal University of Technology – Paraná (UTFPR), Curitiba-PR, Brazil
[3] State University of Maringá, Department of Physics, Maringá-PR, Brazil
[4] Federal University of Technology – Paraná (UTFPR), Medianeira-PR, Brazil
* Corresponding author's e-mail: ctbenatti@uem.br

ABSTRACT

Water treatment plant (WTP) sludge was used as a low-cost adsorbent for manganese (Mn(II)) removal from aqueous solutions. The sludge was subjected to thermal treatment (80–500 °C) and chemical activation with KOH to enhance its physicochemical properties. The activated material exhibited increased porosity and surface functionality, reaching a maximum specific surface area of 191.29 m²/g. Batch adsorption experiments were performed to evaluate the effects of pH, contact time, temperature, adsorbent dosage, and initial Mn concentration. Mn removal was strongly influenced by pH and contact time, with improved performance under alkaline conditions. Adsorption equilibrium was best described by Langmuir model, indicating monolayer adsorption, while kinetic data followed a pseudo-second-order model, suggesting chemisorption as the rate-limiting step. The maximum adsorption capacity reached 0.35 mg/g. Leaching tests demonstrated low release of aluminum, iron, and manganese, confirming the environmental safety of the material. Although the adsorption capacity is moderate, the results highlight the potential of WTP sludge as a sustainable alternative for Mn removal, supporting circular economy principles.

Keywords: water treatment sludge, waste valorization, thermal-chemical activation, adsorption, manganese removal.

INTRODUCTION

The global demand for drinking water has increased markedly over recent decades, driven by population increase, urbanization, industrial growth, intensive agriculture, and climate variability (Das and Mishra, 2025). Water demand has increased substantially due to population growth and urbanization, placing increasing pressure on existing water supply systems and available water resources (Mapani et al., 2023). In addition, urban water quality has deteriorated due to intensified anthropogenic activities, leading to the widespread detection of a variety of substances, including nutrients, chemicals, emerging contaminants, and pathogens in surface and groundwater sources (Liu et al., 2024; Varatharajan et al., 2025).

Water treatment plants (WTPs) generate significant amounts of sludge during coagulation, sedimentation, and filtration processes used to produce drinking water. Global sludge production exceeds 10,000 t/day, and its quantity and characteristics depend on raw water quality and treatment conditions (Mahanna et al., 2024). Composed primarily of metal hydroxides, mineral particles, natural organic matter, and residual treatment chemicals, this residue is increasingly recognized as a potential secondary resource rather than a waste material (Sousa, Bernardo, Matos, et al., 2025). However, inadequate disposal practices remain common in many regions,

creating environmental and operational challenges associated with sludge management (Hussein et al., 2021). These concerns have stimulated research on sludge reuse and valorization pathways aligned with circular economy principles (Truong et al., 2021).

In response, several valorization strategies for WTP sludge have been investigated, including coagulant recovery (Truong et al., 2021; Nomanifar et al., 2024), incorporation into construction materials (Mahanna et al., 2024; Mattoso et al., 2024; Li et al., 2025), soil amendment (Ribeiro et al., 2022), and use in constructed wetlands (Hernández-Crespo et al., 2022). More recently, the conversion of WTP sludge into value-added adsorbent materials has emerged as a promising route within circular economy frameworks (Nguyen et al., 2022; Almeida et al., 2024). The mineralogical composition of WTP sludge, typically rich in aluminum oxides, iron oxides, and silica, confers physicochemical properties that favor adsorption processes, including surface charge variability and affinity for a range of aqueous contaminants (Wu et al., 2004; Zhao et al., 2021). Adsorption has attracted considerable attention due to its high efficiency, versatility, and cost-effectiveness, particularly when low-cost adsorbents derived from waste materials are employed (Akhtar et al., 2025; Nishi et al., 2025).

Among contaminants of concern in drinking water systems, manganese (Mn) warrants particular attention due to its widespread occurrence and challenges of its removal. In aqueous environments, Mn predominantly exists as Mn^{2+} under reducing conditions, remaining soluble and difficult to remove by conventional treatment processes (Chen, 2018). Under oxidizing conditions, Mn^{2+} may form insoluble Mn(III) and Mn(IV) oxides, causing turbidity, discoloration, and operational issues in distribution systems (Tobiason et al., 2016). Although essential at low concentrations, chronic exposure to elevated Mn levels has been associated with neurotoxic effects and cognitive impairment, particularly in children (Rumsby et al., 2014; Aiken et al., 2023). Conventional treatment processes are often insufficient for effective Mn removal, requiring additional physical, chemical, or biological steps that may increase operational complexity and costs (Pearl et al., 2025; Riad, 2025).

Although several studies have explored WTP sludge-derived adsorbents for fluoride, phosphate, nitrate, dyes and organic contaminants (Abo-El-Enein et al., 2017; Almeida et al., 2024; Akhtar et al., 2025), studies specifically focused on Mn(II) adsorption remain scarce. To the best of our knowledge, no previous study has evaluated the combined effects of thermal treatment and KOH activation of WTP sludge for Mn(II) removal while linking physicochemical modifications, pH_{PZC}, porosity development and adsorption performance.

In this context, adsorption has gained increasing attention as a promising approach for Mn removal (Wu et al., 2004). WTP sludge-derived adsorbents have been successfully applied for the removal of anionic contaminants such as nitrate and fluoride, with removal efficiencies depending on the treatment and activation methods employed (Zhang et al., 2015; Phan Quang et al., 2022; Letshwenyo et al., 2023). However, despite isolated reports of manganese removal in multi-contaminant systems, investigations specifically targeting Mn adsorption using WTP sludge remain limited. This gap is particularly relevant given the need for cost-effective and sustainable solutions for manganese control in drinking water systems, while also supporting the valorization of WTP sludge as a resource within circular economy frameworks.

In this context, the present study investigates the production and characterization of adsorbents derived from WTP sludge subjected to thermal treatment and chemical activation with KOH and evaluates their performance in Mn(II) removal from aqueous solutions. The relationship between activation, material properties, and adsorption performance is examined to advance the development of waste-derived adsorbents for water treatment applications, supporting resource recovery and valorization strategies within a circular economy framework.

MATERIALS AND METHODS

Sludge sampling

Sludge was collected from the Maringá drinking WTP (Paraná, Brazil) in September 2023. The facility operates a conventional treatment process, including coagulation with polyaluminum chloride. Samples were collected from a high-rate clarifier during routine cleaning and sludge withdrawal operation. The sludge was thickened in a drainage bed lined with geotextile fabric,

sun-dried for 4 hours, fragmented, and sieved (2.00–2.36 mm) according to ABNT NBR NM ISO 3310-1 (ABNT, 2010), with the 2.00 mm fraction selected for subsequent analysis. Thermal treatments were performed in a muffle furnace (80, 200, and 500 °C) to promote gradual organic matter removal and structural modification, and designated as in natura, 80, 200, and 500.

The thermally treated sample at 500 °C was chemically activated with 0.5 mol/L KOH (analytical grade, Êxodo Científica) and designated as 500 + KOH. Activation was performed with 1 g of adsorbent in 100 mL of KOH solution under agitation in a Dubnoff shaking water bath for 6 h at room temperature. Subsequently, the sample was filtered through qualitative filter paper (80 g/m²), dried at 80 °C for 24 h, washed with ultrapure water, and treated with 0.1 mol/L HCl (analytical grade, Fmaia) for 30 min. The material was rinsed to neutral pH and dried at 105 °C until complete moisture removal (Oumabady et al., 2021).

Sludge characterization

Total solids (TS), fixed solids (FS), and volatile solids (VS) of in natura sludge were determined according to Standard Methods (Methods 2540-B and 2540-E) and Brazilian standard NBR 10664 (ABNT, 1989; APHA/AWWA/WEF, 2017).

Thermogravimetric analysis (TG/DTG) was performed using a PerkinElmer STA 6000 with 10 mg samples, heated from 100 to 800 °C at 20 °C/min under synthetic air (20 mL/min). DTG curve was obtained from TG to identify decomposition temperatures and thermal stability ranges.

Particle size distribution was determined by laser diffraction (Bettersizer S2 WD) using aqueous dispersion with pyrophosphate. Samples (6–10 g) were homogenized and analyzed by activation temperature, with system cleaned between runs. D10, D50, and D90 represent fine fraction, median diameter, and coarse fraction, respectively (Islam et al., 2022).

pH at point of zero charge (pH_{PZC}) was determined by the 11-point method (1995) using 0.025 g of adsorbent in 100 mL of solution (initial pH 2–12), agitated for 24 h at 25 °C. The pH_{PZC} corresponds to the pH range where final pH is independent of the initial value.

Fourier transform infrared spectroscopy (FTIR) was conducted using an Avatar 360-FTIR spectrometer (Thermo Nicolet) over 4000–400 1/cm to determine structural characteristics.

X-ray diffraction (XRD) was employed using a Bruker D8 Advance diffractometer (Co radiation, 40 kV, 30 mA), scanning 10–110° (2θ) at 0.02° steps and 2°/min to identify crystalline phases and structural changes.

Nitrogen physisorption (Linde, >99.999%) at 77 K (1.2×10^{-3}–0.092 MPa) was performed using a Micromeritics ASAP 2020 to determine specific surface area. Before analysis, samples were degassed at 1.3×10^{-4} MPa and 150 °C with a heating rate of 5 °C/min for 3 h. Specific surface area was calculated by BET equation (Brunauer et al., 1938), and total pore volume estimated at $P/P_0 = 1$.

Surface area and pore size distribution were obtained from N_2 adsorption–desorption isotherms at 77 K using an Autosorb analyzer (Quantachrome). The BET specific surface area was calculated using the Brunauer–Emmett–Teller equation (Brunauer et al., 1938), while pore size distribution, pore volume, and average pore diameter were determined using the Horváth–Kawazoe (HK) method (Horváth and Kawazoe, 1983). Micropore surface area was estimated using the Halsey t-plot method (Gregg et al., 1967).

Morphology was analyzed by scanning electron microscopy (SEM), and elemental composition was determined by energy-dispersive X-ray spectroscopy (EDS) using a Zeiss EVO MA15 microscope equipped with an Oxford X-Max 20 mm² detector after gold sputter coating.

Leaking tests of the sludge-derived adsorbents

Leaching tests were conducted to assess the environmental safety of the adsorbents, focusing on the major elements present in the sludge (Al, Fe, and Mn), following Methods No. 13 and No. 46 of the Japanese Ministry of the Environment (Zhang and Itoh, 2003). Samples (1 g) of raw and thermally treated materials (80, 200, and 500 °C) were leached in 100 mL of ultrapure water at pH 5, 7, and 9, adjusted with 0.1 mol/L HCl or NaOH. The suspensions were agitated (~50 rpm) for 6 h at room temperature using a Dubnoff bath. Aluminum (APHA/AWWA/WEF, 2017), iron (Stookey, 1970), and manganese (DIN Deutsches Inst. fuer Normung, 2024) concentrations were determined by UV–Vis spectrophotometry (Spectroquant Prove 600, Merck) at 570, 510, and 525 nm, respectively.

Evaluation of manganese adsorption using the selected sludge-derived adsorbent

Manganese adsorption studies were conducted using a standard solution (>99% metal, Specsol) prepared in analytical-grade nitric acid (Neon) and diluted with ultrapure water to an initial concentration of 0.42 mg/L, exceeding the drinking water limit of 0.1 mg/L established by Ordinance GM/MS No. 888/2021 (Brazil. Ministry of Health, 2021). This concentration is within the range reported for manganese-contaminated drinking water systems (Friedman et al., 2024). A fractional factorial experimental design with a central point (2^{5-1}) was employed to evaluate the influence of pH, adsorbent dosage, initial concentration, contact time, and temperature on manganese adsorption, according to the levels shown in Table 1.

The equilibrium adsorption capacity (q_e, mg/g) was determined using Equation 1. Statistical analyses were performed using Minitab statistical software (version 1.3.0).

$$q_e = \frac{(C_0 - C_e)V}{m} \quad (1)$$

where: C_0 and C_e (mg/L) are the initial and final Mn concentrations, respectively; V (L) is the volume of the solution; and m (g) is the dry mass of adsorbent.

Manganese adsorption experiments included kinetic and isotherm studies. For the kinetic experiments, 0.5 g of adsorbent was added to 100 mL of Mn solution (0.50 mg/L) at pH 10 under constant agitation at 25 °C. Aliquots were collected at predetermined intervals (0–1440 min) and analyzed by UV–Vis spectrophotometry at 525 nm (Spectroquant Prove 600, Merck), following the DIN standard method (DIN Deutsches Inst. fuer Normung, 2024).

The adsorption capacity at time t (q_t, mg/g) was calculated using Equation 2.

$$q_t = \frac{(C_0 - C_t)V}{m} \quad (2)$$

where: C_t (mg/L) is the Mn concentration at time t (min).

Kinetic data were analyzed using pseudo-first-order and pseudo-second-order models (Belaid et al., 2013; Robati, 2013). The linearized forms of the pseudo-first-order and pseudo-second-order models are presented in Equations 3 and 4, respectively:

$$log\ \log(q_e - q_t) = log q_e - \frac{k_1}{2.303} t \quad (3)$$

$$\frac{t}{q_t} = \frac{1}{k_2 q_e^2} + \frac{1}{q_e} t \quad (4)$$

where: k_1 (1/min) is the pseudo-first-order rate constant and (g/mg min) is the pseudo-second-order rate constant.

For isotherm experiments, Mn concentrations of 0.40, 0.70, and 0.94 mg/L were employed under conditions without pH adjustment. After 1440 min, the supernatant was analyzed by UV–Vis spectrophotometry, and Langmuir and Freundlich models were fitted to the data (Siswoyo et al., 2019). The Langmuir isotherm assumes monolayer adsorption on a homogeneous surface and is described by Equation 5:

$$q_e = \frac{K_L\, C_e}{1 + K_L\, C_e} \quad (5)$$

where: q_{max} (mg/g) is the maximum monolayer adsorption capacity; K_L (L/mg) is the Langmuir affinity constant; and C_e (mg/L) is the equilibrium concentration.

For parameter estimation, the linearized form was applied (Equation 6):

$$\frac{C_e}{q_e} = \frac{1}{q_{max} K_L} + \frac{C_e}{q_{max}} \quad (6)$$

The dimensionless separation factor (R_L) was calculated using Equation 7, where $0 < R_L < 1$ indicates favorable adsorption.

Table 1. Independent variables and their respective levels used in the fractional factorial design (2^{5-1})

Factors	Levels		
	Inferior (-1)	Central (0)	Superior (+1)
pH	4	7	9
Adsorbent dose (g/L)	1	5	10
Mn concentration (mg/L)	0.1	0.3	0.6
Temperature (°C)	25	35	45
Time (h)	0.5	12	24

$$R_L = \frac{1}{1 + K_L C_0} \quad (7)$$

The Freundlich isotherm model, which assumes heterogeneous surface adsorption, is expressed by Equation 8:

$$q_e = K_F\, C_e^{1/n} \quad (8)$$

where: K_F (mg/g)·(L/mg)$^{1/n}$ is the Freundlich adsorption capacity constant and n (dimensionless) is the heterogeneity factor.

The linearized form used for parameter estimation is shown in Equation 9:

$$log\ q_e = log\ K_F + \frac{1}{n} log\ C_e \quad (9)$$

Model adequacy was evaluated using the coefficient of determination (R^2).

RESULTS AND DISCUSSION

Physicochemical and morphological characterization of the obtained adsorbents

The sludge presented 40.02% moisture and 59.98% TS, of which FS accounted for 41.09% (68.51% of TS) and VS for 18.89% (31.48% of TS). Compared to literature values (25–26%) (Ramirez et al., 2018; Santiago Martins et al., 2022), these differences may be attributed to season variation, clarifier retention time, and water source characteristics. Such factors may affect sludge organic matter content, which here exceeds that reported by Santiago Martins et al. (2022) (4.93%), but is lower than the 31% observed by Gonçalves et al. (2017). The considerable organic matter fraction highlights the importance of thermal treatment to enhance material stability and reduce biodegradability.

Particle size distribution analysis (Figure 1) showed that increasing treatment temperature increased D10, D50, and D90). Thermal treatment induces agglomeration and sintering, increasing particle size, as described by Latosińska et al. (2021), reducing the proportion of fine particles and, consequently, surface area and adsorption capacity. Balancing these effects with porosity development is crucial for optimizing adsorption (Godoy et al., 2019). Correlation with BET results (Table 2) indicates that samples treated at 80 °C exhibited lower surface area than those at 200 °C. This is likely due to higher residual moisture and organic matter content in these samples.

Thermal analysis (Figure 2a) revealed three degradation stages: (A) 100–250 °C, gradual phenomenon associated with moisture loss; (B) 250–400 °C, a more pronounced mass loss corresponding to organic matter volatilization and metal oxides dehydration; (C) 400–498 °C, related to structural reorganization and crystallization. Thermal stabilization occurred near 500 °C, consistent with previous studies involving WTP sludge (de Oliveira Silva et al., 2012; Martins et al., 2022) and with Yang et al. (2023), who reported mineralogical stabilization around 450 °C. Therefore, treatment at 500 °C effectively reduces undesirable organic compounds while maintaining the structural integrity of the adsorbent.

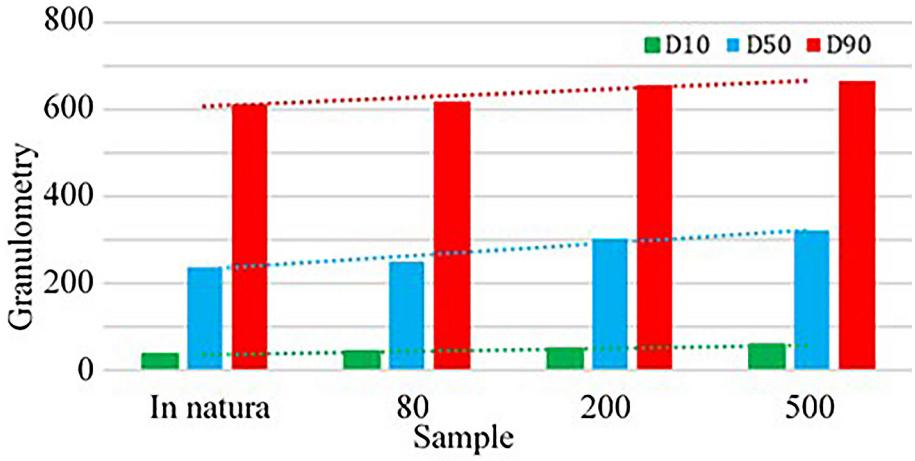

Figure 1. Particle size distribution of the in natura and thermally treated adsorbents at different temperatures (80, 200, and 500 ºC)

Table 2. Surface characteristics of the adsorbents (pH_{PZC} and porosity)

Parameter	Sample				
	In natura	80	200	500	500+KOH
pH_{PZC}	8.84	8.94	8.62	5.41	6.77
BET specific surface area (m^2/g)	141.43	94.68	112.43	80.95	133.01
Langmuir surface area (m^2/g)	207.11	137.39	161.19	116.65	191.29
Micropore volume (cm^3/g)	0.0044	0.0024	0.0118	0.0054	0.0101
Mesopore volume (cm^3/g)	2.3104	0.1823	0.2421	0.2844	0.3509
Macropore volume (cm^3/g)	0.0268	0.0183	0.0198	0.0238	0.0216
Total pore volume (cm^3/g)	2.34	0.20	0.27	0.31	0.38
Average pore diameter (nm)	59.52	7.50	9.38	13.10	12.60
Median pore width (nm)	328.28	18.92	20.28	32.30	36.02

The pH_{PZC} values (Table 2) indicate limited surface modification after treatment at 80 °C and 200 °C. Thermal treatment at 500 °C reduced the pH_{PZC} to 5.41, while KOH activation increased it to 6.77, likely due to hydroxyl groups incorporation, similar to the value reported by Santiago Martins et al. (2022) (6.15). As Mn adsorption is favored above the pH_{PZC}, pH plays a key role in adsorption performance. Since the adsorption experiments were conducted at pH 10, the surface of both adsorbents was predominantly negatively charged. Under these conditions, deprotonation of surface hydroxyl groups generates negatively charged sites that enhance electrostatic attraction toward Mn^{2+} ions, increasing the availability of adsorption sites and favoring manganese uptake from solution. Since adsorption experiments were conducted at pH 10, the contribution of $Mn(OH)_2$ precipitation cannot be completely ruled out. The specific functional groups potentially involved in this mechanism are discussed in the FTIR analysis presented below. Furthermore, the higher pH_{PZC} observed after KOH activation suggests modifications in surface chemistry that may have contributed to the improved adsorption performance of the activated material (Tran et al., 2017; Joseph et al., 2019; Nguyen et al., 2022). Partial ion exchange between Mn^{2+} ions and surface-bound K^+ or H^+ species may also contribute to manganese uptake. In addition to electrostatic attraction, partial ion exchange between Mn^{2+} ions and surface-bound K^+ or H^+ species may also contribute to manganese uptake, particularly after alkaline activation, which can alter the distribution of exchangeable surface ions.

Thermal and chemical treatments significantly affected specific surface area and porosity. Increasing temperature from 80 to 200 °C enhanced specific surface area and pore expansion, whereas treatment at 500 °C reduced surface area due to sintering and micropore collapse despite increased pore dimensions from organic matter degradation, consistent with El-Shorbagy et al. (2025). In contrast, KOH activation increased specific surface area and pore development through carbon–KOH reactions that promote micropore formation and pore widening, in agreement with previous studies (Wang et al., 2021; Ben Ali et al., 2024).

Complementary to the porosity analysis, SEM micrographs of adsorbent samples obtained from treated sludge residue were examined, as presented in Figure 3. SEM images revealed a rough surface and irregular microstructure, consistent with Wang et al. (2021). Increasing temperature favored macropore formation and structural fragmentation, although less pronounced than chemical activation (El-Shorbagy et al., 2025). At 80 °C the material remained compact, whereas at 200 °C, the material presented greater disaggregation and more regular morphology, such as diatom frustules with microperforation patterns (Skubiszewska-Zięba et al., 2012). At 500 °C, collapsed structures with dense agglomerates and fewer active pores were observed, indicating pore loss due to sintering and surface fusion processes (Latosińska et al., 2021; Liu et al., 2025). These observations agree with BET results. The SEM observations are consistent with the BET results and help explain the changes in textural properties induced by thermal and chemical treatment: the sample treated at 500 °C showed a more compact morphology with signs of structural collapse and particle agglomeration, suggesting partial pore shrinkage and loss of accessible surface area, which agrees with the lower BET surface area observed for this material. In contrast, KOH

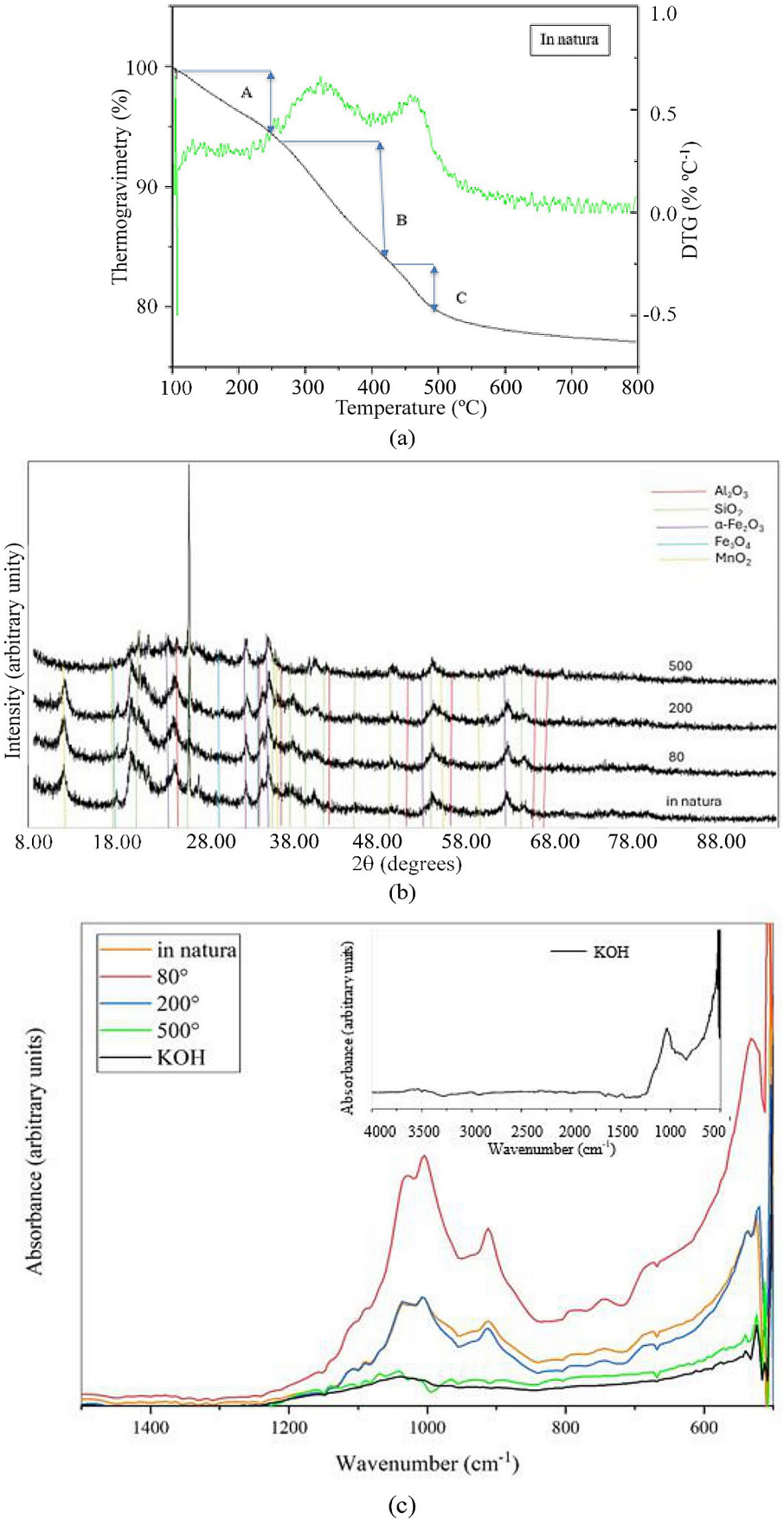

Figure 2. Physicochemical characterization of WTP sludge-derived adsorbents: (a) TG and DTG curves of the in natura sample; (b) X-ray diffraction patterns of raw and thermally treated sludge (80, 200, and 500 °C); and (c) FTIR spectra of treated samples, with the inset showing the O–H band of the KOH-activated material

activation promoted surface etching, particle disaggregation, and the reopening of blocked pores, resulting in a rougher and more porous morphology; these microstructural changes are in good agreement with the increase in BET surface area and pore volume measured for the 500 KOH sample, indicating that alkaline activation enhanced the accessibility of adsorption sites (Tseng and Tseng, 2005; Zhang et al., 2025). Siliceous diatom frustules were detected in all samples, even after thermal treatment, corroborating previous reports (Pookmanee et al., 2011; Skubiszewska-Zięba et al., 2012; Allen et al., 2020).

EDS analysis (Table S1) shows that thermal and chemical treatments altered the elemental composition of the WTP sludge-derived materials. The residue, a by-product of drinking water treatment, is primarily composed of organic matter and treatment reagents and is classified as aluminum-rich (Sousa et al., 2025). The high Fe content is attributed to its natural presence in water sources and regional clay-rich soils (Silva et al., 2025). Carbon content progressively decreased from 15.54% (in natura) to 4.81% after KOH activation, confirming organic matter degradation. Oxygen remained predominant, indicating the prevalence of oxides and minerals (SiO_2, Al_2O_3, Fe_2O_3), which are characteristic of WTP sludge. Aluminum, silicon, and iron contents increased with temperature due to mineral enrichment, with iron rising from 4.30% to 38.66% after activation. Calcium, magnesium, titanium, manganese, and zinc remained as secondary constituents, representing typical impurities in WTP sludge, with little variation. Potassium incorporation confirmed successful KOH treatment, while phosphorus and chlorine detected in some samples are likely associated with residual chemical compounds and may be partially removed during calcination and chemical activation processes. Overall, the material evolved from an organic–mineral matrix rich in carbon and metal oxides (Al, Si, Fe) to a predominantly mineral structure with increased potassium content after alkaline activation. This transformation is typical of activated materials derived from WTP sludge. Elemental analysis confirms enrichment in metal oxides (Si, Al, and Fe) and incorporation of treatment-derived components (K), consistent with Ferreira et al. (2022).

After elemental composition analysis, X-ray diffraction (XRD) (Figure 2b) was used to determine the structural arrangement of phases and assess changes induced by thermal activation.

Peaks at 22° and 27° indicate the presence of quartz (SiO_2), with increased intensity at 27° after treatment at 500 °C suggesting structural modifications induced by heating, consistent with previous studies (Abo-El-Enein et al., 2017; Martins et al., 2022; Bougrine et al., 2024). Quartz is generally regarded as a weakly reactive phase,

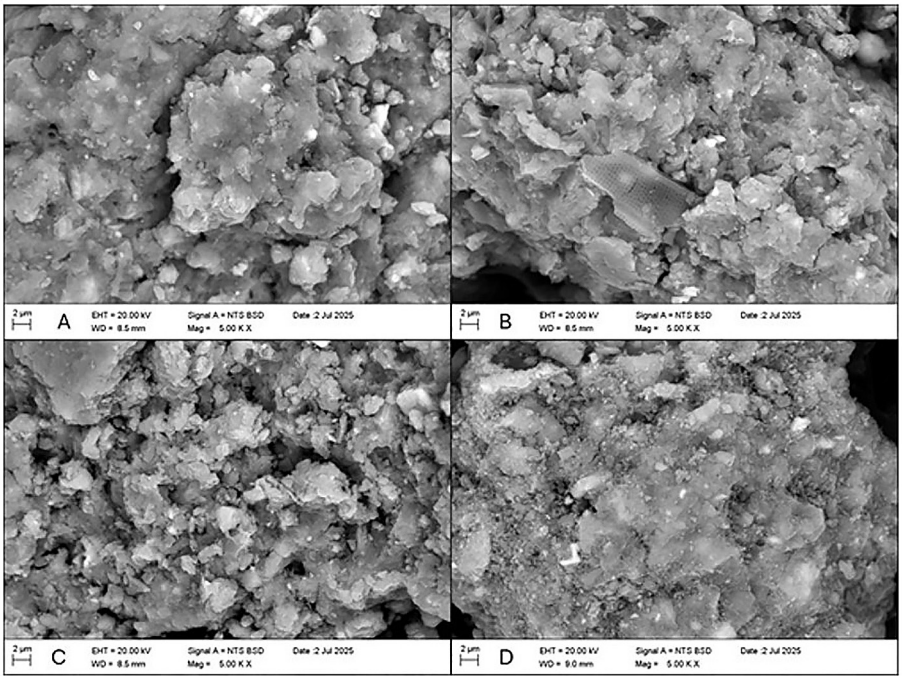

Figure 3. SEM micrographs of adsorbent samples derived from treated sludge residue: (A) 80ºC, (B) 200 °C, (C) 500 °C, and (D) 500 °C and subsequently chemical activated with KOH

contributing mainly to the physical framework of the adsorbent rather than to manganese uptake (Allen et al., 2019). Peaks at 35.5° and 43.4° correspond to Al_2O_3 in the corundum phase, likely from the polyaluminum chloride coagulant. Alumina can participate in manganese removal through surface hydroxyl groups (Al–OH), which may serve as sites for specific complexation under alkaline conditions, although its relative contribution depends on surface hydroxylation and solution chemistry (Micera et al., 1986). Hematite (α-Fe_2O_3) is identified by peaks near 33.2°, 54°, and 63°, while magnetite (Fe_3O_4) appears at 35.4° and 62.5°. Hematite and magnetite likely contribute to manganese removal through surface complexation at Fe–OH sites, in addition to electrostatic interactions. Under alkaline conditions, deprotonation of surface hydroxyl groups increases the density of negatively charged sites, enhancing Mn^{2+} uptake by specific adsorption onto iron oxide phases(Morgan & Stumm, 1964; Gadde and Laitinen, 1974). Additionally, peaks around 8° and 12° in the activated samples suggest the presence of birnessite-like MnO_2. This is a highly significant finding, since birnessite is widely recognized as one of the most efficient natural Mn scavengers, capable of removing Mn^{2+} not only by adsorption but also by surface-catalyzed oxidation and subsequent incorporation into the oxide structure. Therefore, its formation may represent a key mechanism underlying the improved manganese uptake observed after activation (Bruins et al., 2015). These phases reflect both the regional mineralogy and structural modifications induced by thermal and chemical treatments.

The samples were also analyzed by Fourier transform infrared spectroscopy (FTIR) (Figure 2c). Partial spectra (400–1500 1/cm) of the samples treated at different temperatures are presented due to the absence of significant signals in other regions, whereas the full FTIR spectrum of the KOH-treated sample is highlighted, showing distinct O–H bands (4000–3000 1/cm). These results enable identification of functional groups and their evolution with thermal and chemical treatment. Peaks at 1036–1004 1/cm correspond to C–O bonds, indicating organic matter (Kowalski et al., 2018; Martins et al., 2022), with intensity progressively decreasing as temperature increases. The peak at 912 1/cm is associated with Al–OH stretching and Si–O–Si structures (Martins et al., 2022; Figueira et al., 2025). The signal at 535 1/cm is attributed to metal oxides, including Al–O bands in amorphous aluminum oxide or hydroxide phases, Fe–O vibrations, and bands related to O–H groups and manganese oxides (Zhang et al., 2015; Abdel-Ghani et al., 2016; Gao et al., 2024). Bands in the 3000–3250 1/cm region in the KOH-treated sample indicate the presence of O–H groups (Kassem et al., 2023).

Manganese removal using the prepared adsorbent

The prepared adsorbents were evaluated for manganese removal from aqueous solution. Chemical activation with KOH significantly enhanced adsorption, whereas thermally treated adsorbents without chemical activation exhibited manganese leaching originating from their intrinsic composition. The highest performance was achieved by the sample 500 + KOH after 48 h of contact time, reaching 64% removal (0.025 mg/g), with reduced aluminum, iron, and manganese leaching (Table S2). Therefore, this condition was therefore selected for further adsorption studies.

Previous studies indicate that Mn removal cannot be explained solely by stoichiometry (Morgan and Stumm, 1964; Tobiason et al., 2016), as manganese oxides formed by the oxidation of Mn on the adsorbent surface can further adsorb Mn^{2+} ions through ion-exchange mechanisms, during which H^+ ions are released into the solution (Gadde and Laitinen, 1974; Rahman et al., 2021).

The fractional factorial experimental design results (Table S3) identified adsorbent dosage, initial Mn concentration, contact time, pH, and temperature as significant factors affecting Mn removal by the sample 500 + KOH ($p < 0.05$). The high F-value obtained for the model (479.49) indicates that the variability explained by the tested factors greatly exceeds random variation, confirming their significant influence on the response. The model p-value was 0.036, indicating statistical significance at the 5% level. Significant effects were also observed for pH, Mn concentration, temperature, and contact time, as well as for the interaction terms pH × Mn concentration, pH × time, and time × temperature.

The Pareto chart (Figure 4a) ranked contact time and initial Mn concentration as the most influential variables, followed by the interaction effects pH × Mn concentration and pH × contact time. Factors below the significance threshold

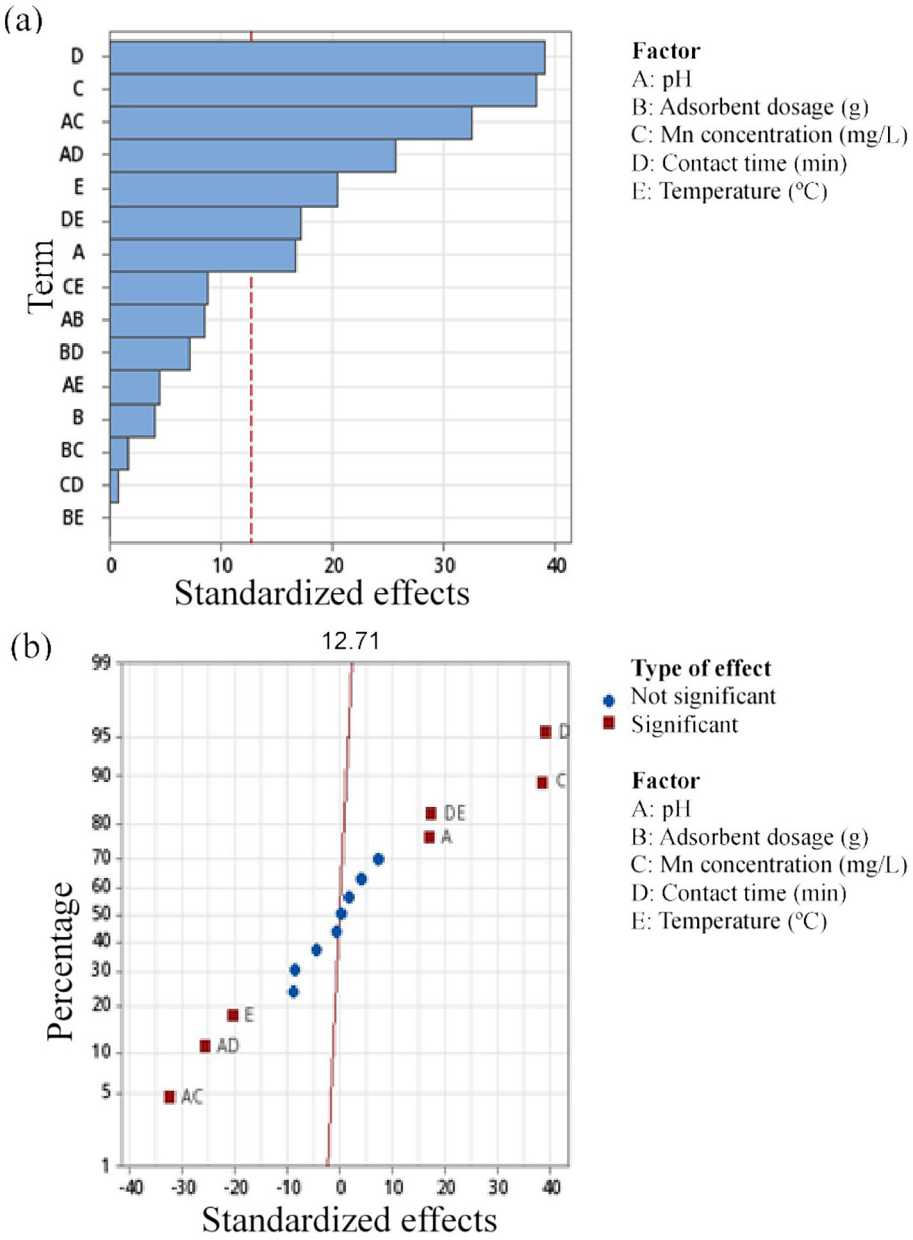

Figure 4. Pareto chart (a) and normal probability plot (b) of standardized effects for the adsorbent treated at 500 °C and activated with KOH

were not statistically relevant. The normal probability plot (Figure 4b) confirmed these findings, with significant factors deviating most from zero. Positive effects indicate increased adsorption efficiency with increasing pH, Mn concentration, and contact time, whereas temperature exhibited a negative effect.

Adsorption kinetics (Figure 5) were evaluated to elucidate mass transfer mechanisms and determine the equilibrium time of Mn uptake by the KOH-activated sludge treated at 500 °C. Based on the factorial design results, pH 10 was selected as the optimal condition for the detailed kinetic investigation.

Kinetic profile shows that the amount of adsorbed manganese (q_e) increases rapidly during the initial contact period, reaching approximately 0.025 mg/g within the first 120 min, indicating a fast adsorption stage. After this period, the adsorption rate gradually decreases and approaches equilibrium. At around 1440 min, reaches approximately 0.040 mg/g, suggesting saturation of the active sites and establishment of adsorption equilibrium. This behavior is typical of adsorption processes in which surface site availability governs the initial uptake, while intraparticle diffusion becomes rate-limiting at later stages (Tran et al., 2018).

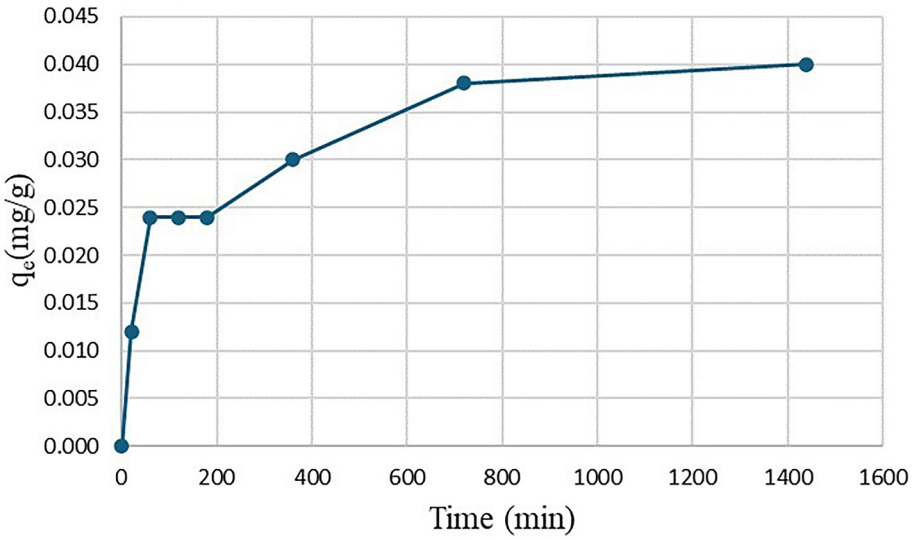

Figure 5. Mn adsorption capacity as a function of contact time for the adsorbent treated at 500 °C and activated with KOH

The 500 + KOH material exhibited a maximum adsorption capacity of 0.025 mg/g, increasing to approximately 0.040 mg/g after 1440 min, which is lower than the values reported for several inorganic waste-based adsorbents. For example, mining wastes such as magnetic tailings, flotation tailings, and sludge showed better adsorption potential for manganese, particularly the sludge fraction, when tested with 30 mg of adsorbent in 10 mL of a 2 mg/L Mn solution (Mendes and Alves, 2024). Sewage sludge ash reached an adsorption capacity of approximately 0.639 mg/g for Mn^{2+} removal under the conditions of 10 mg/L Mn^{2+} and 10 g/L adsorbent (İrdemez et al., 2022). Fly ash also demonstrated relevant performance, with adsorption capacities of about 0.031 mg/g at pH 3.0 and 0.069 mg/g at pH 8.5, reflecting the strong effect of alkaline conditions on manganese removal (Sharma et al., 2007). Overall, these results indicate that waste-derived inorganic materials generally outperform the 500 + KOH sample, likely due to their richer mineral composition, higher density of reactive surface sites, and greater sensitivity to pH

Pseudo-first-order and pseudo-second-order models were fitted to the experimental data, and the corresponding kinetic parameters are presented in Table S4. The pseudo-second-order model provided the best fit to the manganese adsorption kinetics, as indicated by the highest R^2 value. The adsorption capacity predicted by the model (q_e) was 0.044 mg/g. This result suggests that chemisorption is likely the rate-controlling step in the adsorption mechanism of manganese onto the WTP sludge-derived adsorbent treated at 500 °C and activated with KOH, consistent with the findings reported by Mendes and Alves (2024) and Geremias et al. (2012). The kinetic analysis allowed determination of the equilibrium time, while the isotherm parameters (Table 3) provide insights into the maximum adsorption capacity and the nature of the adsorbate–adsorbent interactions, enabling a comprehensive evaluation of system behavior under different experimental conditions.

The Langmuir model showed the best fit to the experimental data, with a coefficient of determination (R^2) of 0.943, indicating strong agreement between predicted and observed values. The estimated maximum adsorption capacity q_{max} was 0.350 mg/g, while the Langmuir constant (K_L = 0.086 L/mg) suggests moderate affinity between the adsorbent and manganese ions. The separation factor (R_L = 0.971), close to unity, indicates

Table 3. Parameters obtained for Langmuir and Freundlich model fitting

Parameter	Langmuir model				Freundlich model		
	q_{max}	K_L	R_L	R^2	n	K_F	R^2
Sample|Unity	mg/g	L/mg	-	-	-	(mg/g)(L/mg)$^{1/n}$	-
500 + KOH	0.350	0.086	0.971	0.943	2.281	0.065	0.888

favorable adsorption with near-linear characteristics (Piccin et al., 2011; Nandiyanto et al., 2020). Although the Langmuir model predicted a theoretical maximum adsorption capacity of 0.35 mg/g, the experimentally observed uptake under environmentally relevant manganese adsorption capacity was between 0.025 and 0.040 mg/g (Figure 5). This difference may be related to the theoretical nature of the Langmuir maximum adsorption capacity and to the increased uncertainty associated with parameter estimation when isotherm experiments are performed within a relatively low concentration range (Fallou et al., 2016).

The Freundlich model also adequately described the system (R^2 = 0.8884), although with lower correlation than Langmuir. The value of n (2.281) greater than 1 confirms favorable adsorption, while 1/n (0.438) indicates moderate surface heterogeneity. The Freundlich constant K_F (0.065) reflects adsorption capacity at low solute concentrations (Piccin et al., 2011).

Overall, the results indicate that Mn adsorption is better described by the Langmuir model, suggesting predominant monolayer formation on relatively homogeneous active sites, although the Freundlich parameters confirm some degree of surface heterogeneity. The favorable n and R_L values corroborate the suitability of the adsorbent treated at 500 °C and activated with KOH. Similar behavior has been reported for WTP sludge-derived materials in previous studies (Zhang et al., 2015; Li et al., 2018; Vitorette et al., 2022). These results are consistent with adsorption being the primary removal mechanism. Although the experiments were conducted at pH 10, where $Mn(OH)_2$ precipitation may occur, the satisfactory fit of the Langmuir isotherm and pseudo-second-order kinetic model suggests that adsorption was likely the dominant mechanism, although simultaneous surface precipitation may have occurred.

As shown in Table 4, the adsorption capacity obtained in this study is lower than that reported for several engineered adsorbents. However, direct comparison should be interpreted with caution because adsorption capacities are strongly influenced by experimental conditions, particularly the initial metal concentration. Most studies reported in the literature employed Mn(II) concentrations ranging from 5 to 1000 mg/L (Pahade and Sharma, 2015), whereas the present study evaluated adsorption under environmentally relevant concentrations below 1 mg/L. Under such conditions, fewer adsorption sites are occupied, resulting in lower apparent adsorption capacities (Bosco et al., 2006). Therefore, the relatively modest q_{max} value observed here should be interpreted considering the low manganese concentrations investigated and the intended application of the material for water treatment scenarios involving trace-level contamination. Although the adsorption capacity is modest, studies evaluating Mn(II) removal using KOH-activated WTP sludge are scarce, making direct comparison difficult and highlighting the novelty of the present work.

However, it is important to emphasize that the primary objective of this work was to evaluate the feasibility of valorizing water treatment plant sludge as a functional adsorbent. According to Nishi et al. (2025), WTP sludge may be classified as a low-cost adsorbent, for which moderate adsorption capacities can still be considered relevant when associated with environmental and economic advantages. The conversion of WTP sludge into adsorbent material contributes to waste reduction, decreases the burden of sludge disposal, and aligns with circular economy principles by transforming an abundant residual by-product into a value-added resource. Therefore, the practical significance of the material should not be assessed solely based on its adsorption

Table 4. Comparison of Mn(II) adsorption capacities reported for different adsorbents

Adsorbent	Initial Mn concentration (mg/L)	Maximum adsorption capacity (mg/g)	q_{max} (mg/g)	Reference
Modified clays	50–1000	1.24–4.48	4.8	Bosco et al., 2006
Chicken eggs shell	5-100	0.125-4.54	0.639	Altameemi and Thuraya, 2021
Aloe Vera adsorbent	100	45.12	21.123	Sivalingam and Gopal, 2024
Macrophyte *S. polyrhiza*	30	29.0	35.7	Meitei and Prasad, 2014
Black carrot (*Daucus carota L.*) residues	400.0	3.86	3.87	Güzel et al., 2008
Kaolinite	10.0	0.45	0.446	Yavuz et al., 2003
Water treatment sludge	0.1-0.6	0.04	0.35	This study

capacity, but also considering its environmental viability, economic accessibility, and contribution to sustainable resource management.

The favorable adsorption performance, combined with the absence of manganese leaching and low release of aluminum and iron observed in safety tests, confirms the potential of the selected adsorbent (treated at 500 °C and activated with KOH) for water treatment applications. The low tendency for secondary metal release ensures both effectiveness and environmental safety in compliance with Brazilian drinking water standards (Ordinance GM/MS No. 888/2021). These findings demonstrate that WTP sludge can be effectively valorized for the removal of specific contaminants, contributing to waste reduction and water pollution control while supporting sustainable urban water management.

Furthermore, the valorization of WTP sludge, a highly abundant waste generated in thousands of tons Monthly, as a functional adsorbent not only mitigates the environmental impacts of improper disposal but also exemplifies the transition to a circular economy, converting a liability into an active solution for contaminated water treatment. Low-cost adsorbents derived from such residues often surpass commercial alternatives in terms of sustainability and cost-effectiveness, paving the way for scalable industrial applications and promoting sustainable development in urban water supply systems.

CONCLUSIONS

This study demonstrated that WTP sludge, after thermal treatment and chemical activation with KOH, can be effectively transformed into a promising adsorbent for Mn removal from aqueous solutions. Integrated characterization by thermogravimetry, XRD, FTIR, particle size analysis, and BET/Langmuir surface area measurements confirmed the structural and chemical modifications responsible for the enhanced adsorption performance.

Chemical activation with KOH played a crucial role in increasing surface area and porosity, promoting the development of micropores and adsorption channels. Isotherm analysis showed that the Langmuir model provided the best fit, indicating predominant monolayer adsorption with strong affinity for Mn(II), whereas the kinetic data followed the pseudo-second-order model, suggesting chemisorption as the rate-limiting mechanism.

The rapid initial uptake followed by gradual stabilization reflects active site saturation and the contribution of intraparticle diffusion at later stages. FTIR analysis confirmed the presence of functional groups relevant to adsorption (O–H, C–O, Al–OH), and XRD results demonstrated mineralogical stability after treatment. The shift in pH_{PZC} significantly influenced electrostatic interactions, directly affecting Mn adsorption performance.

Importantly, negligible Mn leaching and low aluminum and iron release confirm the environmental safety of the material. Overall, the findings highlight the potential valorization of WTP sludge as a sustainable adsorbent for targeted contaminant removal, contributing to waste reduction and water pollution mitigation in alignment with circular economy principles. Nevertheless, further modifications are required to improve the removal efficiency of anionic contaminants and broaden the material's applicability.

Acknowledgments

The authors would like to thank the Multi-User Material Characterization Center (CMCM) – UTFPR, for helping with SEM analyses.

This study was financed in part by the Coordenação de Aperfeiçoamento de Pessoal de Nível Superior – Brasil (CAPES) – Finance Code 001."

REFERENCES

1. Abdel-Ghani, N.T., El-Chaghaby, G.A., ElGammal, M.H., Rawash, E.-S.A. (2016) Optimizing the preparation conditions of activated carbons from olive cake using KOH activation. *New Carbon Materials*. *31*(5), 492–500. https://doi.org/10.1016/S1872-5805(16)60027-6
2. ABNT (1989) ABNT NBR 10664 Águas - Determinação de resíduos (sólidos) - Método gravimétrico - Método de ensaio.
3. ABNT (2010) NBR NM ISO 3310-1: Test sieves — Technical requirements and testing — Part 1: Test sieves of metal wire cloth.
4. Abo-El-Enein, S.A., Shebl, A., Abo El-Dahab, S.A. (2017) Drinking water treatment sludge as an efficient adsorbent for heavy metals removal. *Applied Clay Science*. *146*, 343–349. https://doi.org/10.1016/j.clay.2017.06.027

5. Aiken, M.L., Pace, C.E., Ramachandran, M., Schwabe, K.A., Ajami, H., Link, B.G., Ying, S.C. (2023) Disparities in drinking water manganese concentrations in domestic wells and community water systems in the Central Valley, CA, USA. *Environmental Science & Technology*. *57*(5), 1987–1996. https://doi.org/10.1021/acs.est.2c08548
6. Akhtar, M., Sarfraz, M., Ahmad, M., Raza, N., Zhang, L. (2025) Use of low-cost adsorbent for waste water treatment: Recent progress, new trend and future perspectives. *Desalination and Water Treatment*. *321*, 100914. https://doi.org/10.1016/j.dwt.2024.100914
7. Allen, C.S., Thomas, E.R., Blagbrough, H., Tetzner, D.R., Warren, R.A., Ludlow, E.C., Bracegirdle, T.J. (2020) Preliminary evidence for the role played by south westerly wind strength on the marine diatom content of an Antarctic Peninsula ice core (1980–2010). *Geosciences*. *10*(3), 87. https://doi.org/10.3390/geosciences10030087
8. Allen, N., Dai, C., Hu, Y., Kubicki, J.D., Kabengi, N. (2019) Adsorption study of $Al^{3+,}$ Cr^{3+}, and Mn^{2+} onto quartz and corundum using flow microcalorimetry, quartz crystal microbalance, and density functional theory. *ACS Earth and Space Chemistry*. *3*(3), 432–441. https://doi.org/10.1021/acsearthspacechem.8b00148
9. Almeida, M.B.G. de, Dantas De Jesus, A.M., Pereira, A.S., Fiore, F.A. (2024) Evaluating centrifuged water treatment plant sludge as an adsorbent for nutrients, microorganisms, and heavy metals removal from wastewater. *Journal of Cleaner Production*. *468*, 142975. https://doi.org/10.1016/j.jclepro.2024.142975
10. Altameemi, I.A., Thuraya, M.A. (2021) Removal of manganese (Mn^{+2}) from aqueous solution by low-cost adsorbents and study the adsorption thermodynamics and kinetics. *Journal of Physics: Conference Series*. *1773*(1), 012038. https://doi.org/10.1088/1742-6596/1773/1/012038
11. APHA/AWWA/WEF (2017) *Standard methods for the examination of water and wastewater*, 23rd ed. American Public Health Association, American Water Works Association, Water Environment Federation, Washington. DC.
12. Belaid, K.D., Kacha, S., Kameche, M., Derriche, Z. (2013) Adsorption kinetics of some textile dyes onto granular activated carbon. *Journal of Environmental Chemical Engineering*. *1*(3), 496–503. https://doi.org/10.1016/j.jece.2013.05.003
13. Ben Ali, M., Flayou, M., Boutarba, Y., El Youssfi, M., Bakhtaoui, Y., El Hazzat, M., Sifou, A., Dahhou, M., et al. (2024) Conversion of urban sludge into KOH-activated biochar for methylene blue adsorption. *Moroccan Journal of Chemistry*. *12*(4), 1852–1869. https://doi.org/10.48317/IMIST.PRSM/MORJCHEM-V12I4.50578
14. Bosco, S.M.D., Jimenez, R.S., Vignado, C., Fontana, J., Geraldo, B., Figueiredo, F.C.A., Mandelli, D., Carvalho, W.A. (2006) Removal of Mn(II) and Cd(II) from wastewaters by natural and modified clays. *Adsorption*. *12*(2), 133–146. https://doi.org/10.1007/s10450-006-0375-1
15. Bougrine, O., El Fellah, I., Kada, I., Rabie, F.A., Lanjri, A.F., Ammari, M., Ben Allal, L. (2024) Advancing circular economy: A study of drinking water sludge for potential uses. *Results in Engineering*. *23*, 102426. https://doi.org/10.1016/j.rineng.2024.102426
16. Brazil. Ministry of Health (2021) Portaria GM/MS Nº 888, de 4 de maio de 2021. Altera o Anexo XX da Portaria de Consolidação GM/MS nº 5, de 28 de setembro de 2017, para dispor sobre os procedimentos de controle e de vigilância da qualidade da água para consumo humano e seu padrão de potab.
17. Bruins, J.H., Petrusevski, B., Slokar, Y.M., Kruithof, J.C., Kennedy, M.D. (2015) Manganese removal from groundwater: characterization of filter media coating. *Desalination and Water Treatment*. *55*(7), 1851–1863. https://doi.org/10.1080/19443994.2014.927802
18. Brunauer, S., Emmett, P.H., Teller, E. (1938) Adsorption of gases in multimolecular layers. *Journal of the American Chemical Society. 60*(2), 309–319. https://doi.org/10.1021/ja01269a023
19. Chen, P. (2018) Manganese metabolism in humans. *Frontiers in Bioscience*. *23*(9), 1655–1679. https://doi.org/10.2741/4665
20. Das, A., Mishra, S. (2025) Smart and sustainable water management: policy, technology, and innovation pathways for resource resilience. *Green Technology, Resilience, and Sustainability*. *5*(1), 5. https://doi.org/10.1007/s44173-025-00022-8
21. DIN Deutsches Inst. fuer Normung, F.R.). N.W., Berlin (Germany (2024) *German standard methods for the examination of water, waste water and sludge: Cations (group E), determination of manganese (E 2)*, Verl. Chemie.
22. El-Shorbagy, H.G., El-Mosalamy, S.E., El-Sayed, G.O., Metwaly, T.S. (2025) Thermally activated sludge utilization for removal of nickel pollution from aqueous medium. *Thermal Advances*. *3*, 100036. https://doi.org/10.1016/j.thradv.2025.100036
23. Fallou, H., Cimetière, N., Giraudet, S., Wolbert, D., Le Cloirec, P. (2016) Adsorption of pharmaceuticals onto activated carbon fiber cloths – Modeling and extrapolation of adsorption isotherms at very low concentrations. *Journal of Environmental Management*. *166*, 544–555. https://doi.org/10.1016/j.jenvman.2015.10.056
24. Ferreira, G., Barbosa, K.T., Quadro, M.S., Trindade,

G.H., Beltrame, R., Morselli, L.B.G.A., Andreazza, R. (2022) Emprego do lodo de uma estação de tratamento de água beneficiado como material suplementar ao cimento Portland. *Engenharia Sanitaria e Ambiental*. *27*(4), 653–661. https://doi.org/10.1590/s1413-415220210035

25. Figueira, B.A.M., Silva, J.A.S., Nascimento, R.S., Santos, G.R., Campos, A.G.A., Costa, M.L., Freire, P.T.C. (2025) FTIR and Raman spectroscopic characterization of anionic clays obtained from bauxite tailings (Amazon, Brazil). *Materials Research*. 28(suppl 1), e20250229. https://doi.org/10.1590/1980-5373-mr-2025-0229
26. Friedman, A., Boselli, E., Ogneva-Himmelberger, Y., Heiger-Bernays, W., Brochu, P., Burgess, M., Schildroth, S., Denehy, A., et al. (2024) Manganese in residential drinking water from a community-initiated case study in Massachusetts. *Journal of Exposure Science & Environmental Epidemiology*. 34(1), 58–67. https://doi.org/10.1038/s41370-023-00563-9
27. Gadde, R.Rao., Laitinen, H.A. (1974) Heavy metal adsorption by hydrous iron and manganese oxides. *Analytical Chemistry*. *46*(13), 2022–2026. https://doi.org/10.1021/ac60349a004
28. Gao, Y., Liu, S., Zhou, Y., Zhang, J., Zhang, Y. (2024) Adsorption of fluoride by using sodium alginate coated poly-aluminium chloride (PAC) sludge: preparation, characterisation and mechanism. *International Journal of Environmental Analytical Chemistry*. *104*(11), 2534–2551. https://doi.org/10.1080/03067319.2022.2064749
29. Geremias, R., Laus, R., Fávere, V.T. de, Pedrosa, R.C. (2012) Adsorção de íons Cu (II), Mn (II), Zn (II) e Fe (III), utilizando rejeito de mineração de carvão como adsorvente. *Revista Brasileira de Ciências Ambientais*. (25), 48–59.
30. Godoy, L.G.G.D., Rohden, A.B., Garcez, M.R., Costa, E.B.D., Da Dalt, S., Andrade, J.J.D.O. (2019) Valorization of water treatment sludge waste by application as supplementary cementitious material. *Construction and Building Materials*. 223, 939–950. https://doi.org/10.1016/j.conbuildmat.2019.07.333
31. Gonçalves, F., Souza, C.H.U.D., Tahira, F.S., Fernandes, F., Teixeira, R.S. (2017) Incremento de lodo de ETA em barreiras ipermeabilizantes de aterro sanitário. *Revista DAE*. *65*(205), 5–14. https://doi.org/10.4322/dae.2016.018
32. Gregg, S.J., Sing, K.S.W., Salzberg, H.W. (1967) Adsorption surface area and porosity. *Journal of The Electrochemical Society*. *114*(11), 279Ca. https://doi.org/10.1149/1.2426447
33. Güzel, F., Yakut, H., Topal, G. (2008) Determination of kinetic and equilibrium parameters of the batch adsorption of Mn(II), Co(II), Ni(II) and Cu(II) from aqueous solution by black carrot (*Daucus carota* L.) residues. *Journal of Hazardous Materials*. *153*(3), 1275–1287. https://doi.org/10.1016/j.jhazmat.2007.09.087
34. Hernández-Crespo, C., Oliver, N., Peña, M., Añó, M., Martín, M. (2022) Valorisation of drinking water treatment sludge as substrate in subsurface flow constructed wetlands for upgrading treated wastewater. *Process Safety and Environmental Protection*. *158*, 486–494. https://doi.org/10.1016/j.psep.2021.12.035
35. Horváth, G. & Kawazoe, K. (1983). Method for the calculation of effective pore size distribution in molecular sieve carbon. *Journal of Chemical Engineering of Japan*. *16*(6), 470–475. https://doi.org/10.1252/jcej.16.470
36. Hussein, A.M., Mahmoud, R.K., Sillanpää, M., Abdel Wahed, M.S.M. (2021) Impacts alum DWTPs sludge discharge and changes in flow regime of the Nile River on the quality of surface water and cultivated soils in Fayoum watershed, Egypt. *Science of The Total Environment*. *766,* 144333. https://doi.org/10.1016/j.scitotenv.2020.144333
37. İrdemez, Ş., Yeşilyurt, D., Ekmekyapar Torun, F., Kul, S., Bingül, Z. (2022) Investigation of manganese ion removal from waters using sewage sludge ash. *Iranian Journal of Chemistry and Chemical Engineering*. *41*(9), 2972–2985. https://doi.org/10.30492/ijcce.2021.527060.4639
38. Islam, S.F., Hawkins, S.M., Meyer, J.L.L., Sharman, A.R.C. (2022) Evaluation of different particle size distribution and morphology characterization techniques. *Additive Manufacturing Letters*. *3*, 100077. https://doi.org/10.1016/j.addlet.2022.100077
39. Joseph, L., Jun, B.-M., Flora, J.R.V., Park, C.M., Yoon, Y. (2019) Removal of heavy metals from water sources in the developing world using low-cost materials: A review. *Chemosphere*. *229*, 142–159. https://doi.org/10.1016/j.chemosphere.2019.04.198
40. Kassem, A., Abbas, L., Coutinho, O., Opara, S., Najaf, H., Kasperek, D., Pokhrel, K., Li, X., et al. (2023) Applications of Fourier transform-infrared spectroscopy in microbial cell biology and environmental microbiology: advances, challenges, and future perspectives. *Frontiers in Microbiology*. *14*. https://doi.org/10.3389/fmicb.2023.1304081
41. Kowalski, M., Kowalska, K., Wiszniowski, J., Turek-Szytow, J. (2018) Qualitative analysis of activated sludge using FT-IR technique. *Chemical Papers*. *72*(11), 2699–2706. https://doi.org/10.1007/s11696-018-0514-7
42. Latosińska, J., Żygadło, M., Czapik, P. (2021) The influence of sewage sludge content and sintering temperature on selected properties of lightweight expanded clay aggregate. *Materials*. *14*(12), 3363. https://doi.org/10.3390/ma14123363
43. Letshwenyo, M.W., Machola, K., Mokokwe, G.

(2023) Investigation of water treatment sludge for the treatment of saline water: Batch studies. *Heliyon*. *9*(4), e15040. https://doi.org/10.1016/j.heliyon.2023.e15040

44. Li, P., Sun, F., Dong, Y., Wen, L., Lin, L., Li, X. (2025) Utilization of drinking water treatment sludge with coal fly ash to make permeable bricks for low impact development. *Resources, Conservation and Recycling*. *212*, 107932. https://doi.org/10.1016/j.resconrec.2024.107932
45. Li, Y., Yang, S., Jiang, Q., Fang, J., Wang, W., Wang, Y. (2018) The adsorptive removal of fluoride from aqueous solution by modified sludge: optimization using response surface methodology. *International Journal of Environmental Research and Public Health*. *15*(4), 826. https://doi.org/10.3390/ijerph15040826
46. Liu, J., Liu, H., He, C., Xiao, H., Jin, M., Yao, H. (2025) Correlation between sewage sludge pore structure evolution and water filtration performance: effect of thermal hydrolysis with or without carbonaceous skeleton-assisted. *Water Research*. *268*, 122578. https://doi.org/10.1016/j.watres.2024.122578
47. Liu, Z., Ying, J., He, C., Guan, D., Pan, X., Dai, Y., Gong, B., He, K., et al. (2024) Scarcity and quality risks for future global urban water supply. *Landscape Ecology*. *39*(2), 10. https://doi.org/10.1007/s10980-024-01832-0
48. Mahanna, H., Alaa, A., Salah, H., Tahwia, A.M. (2024) Recycling water treatment sludge into a novel eco-friendly core–shell lightweight aggregate and its application. *Clean Technologies and Environmental Policy*. *26*(8), 2557–2572. https://doi.org/10.1007/s10098-024-02747-9
49. Mapani, B.S., Shikangalah, R.N., Mwetulundila, A.L. (2023) A review on water security and management under climate change conditions, Windhoek, Namibia. *Journal of African Earth Sciences*. *197*, 104749. https://doi.org/10.1016/j.jafrearsci.2022.104749
50. Martins, D.S., Estevam, B.R., Perez, I.D., Américo-Pinheiro, J.H.P., Isique, W.D., Boina, R.F. (2022) Sludge from a water treatment plant as an adsorbent of endocrine disruptors. *Journal of Environmental Chemical Engineering*. *10*(4), 108090. https://doi.org/10.1016/j.jece.2022.108090
51. Mattoso, A.P., Cunha, S., Aguiar, J., Duarte, A., Lemos, H. (2024) Valorization of water treatment sludge for applications in the construction industry: a review. *Materials*. *17*(8), 1824. https://doi.org/10.3390/ma17081824
52. Meitei, M.D., Prasad, M.N.V. (2014) Adsorption of Cu (II), Mn (II) and Zn (II) by *Spirodela polyrhiza* (L.) Schleiden: equilibrium, kinetic and thermodynamic studies. *Ecological Engineering*. *71*, 308–317. https://doi.org/10.1016/j.ecoleng.2014.07.036
53. Mendes, M.V.A., Alves, V.N. (2024) Resíduos de mineração como adsorvente 'eco-friendly' para remoção de íons manganês: cinética e estudos de equilíbrio. *Revista Processos Químicos*. *18*(35), 83–89. https://doi.org/10.19142/rpq.v18i35.723
54. Micera, G., Dallocchio, R., Deiana, S., Gessa, C., Melis, P., Premoli, A. (1986) Manganese (II)-aluminium hydroxide interaction: an ESR study. *Colloids and Surfaces*. *17*(4), 395–400. https://doi.org/10.1016/0166-6622(86)80262-1
55. Morgan, J.J., Stumm, W. (1964) Colloid-chemical properties of manganese dioxide. *Journal of Colloid Science*. *19*(4), 347–359. https://doi.org/10.1016/0095-8522(64)90036-4
56. Nandiyanto, A.B.D., Santiuly Girsang, G.C., Maryanti, R., Ragadhita, R., Anggraeni, S., Fauzi, F.M., Sakinah, P., Astuti, A.P., et al. (2020) Isotherm adsorption characteristics of carbon microparticles prepared from pineapple peel waste. *Communications in Science and Technology*. *5*(1), 31–39. https://doi.org/10.21924/cst.5.1.2020.176
57. Nguyen, M.D., Thomas, M., Surapaneni, A., Moon, E.M., Milne, N.A. (2022) Beneficial reuse of water treatment sludge in the context of circular economy. *Environmental Technology & Innovation*. *28*, 102651. https://doi.org/10.1016/j.eti.2022.102651
58. Nishi, L., Ribeiro, A.C., Paraíso, C.M., Cusioli, D.A.G., Beltran, L.B., Cusioli, L.F., Bergamasco, R. (2025) Low-cost adsorbents for water treatment: a sustainable alternative for pollutant removal. *Processes*. *13*(12), 4088. https://doi.org/10.3390/pr13124088
59. Nomanifar, N., Davoudi, M., Ghorbanian, A., Najafpoor, A.A., Hosseinzadeh, A. (2024) Fe recovery from drinking water treatment sludge for reuse in tannery wastewater treatment: machine learning and statistical modelling. *Journal of Water Process Engineering*. *60*, 105224. https://doi.org/10.1016/j.jwpe.2024.105224
60. de Oliveira Silva, J., Filho, G.R., da Silva Meireles, C., Ribeiro, S.D., Vieira, J.G., da Silva, C.V., Cerqueira, D.A. (2012) Thermal analysis and FTIR studies of sewage sludge produced in treatment plants. The case of sludge in the city of Uberlândia-MG, Brazil. *Thermochimica Acta*. *528*, 72–75. https://doi.org/10.1016/j.tca.2011.11.010
61. Oumabady, S., Selvaraj, P.S., Kamaludeen, S.P.B., Ettiyagounder, P., Suganya, K., R., S.P. (2021) Application of sludge-derived KOH-activated hydrochar in the adsorptive removal of orthophosphate. *RSC Advances*. *11*(12), 6535–6543. https://doi.org/10.1039/D0RA10943F
62. Pahade, V., Sharma, D. (2015) Manganese removal by low cost adsorbent from synthetic wastewater - A review. *International Journal of Engineering*

Research. *4*, 111–114. https://doi.org/10.17950/ijer/v4s3/305

63. Park, J., Regalbuto, J.R. (1995) A simple, accurate determination of oxide PZC and the strong buffering effect of oxide surfaces at incipient wetness. *Journal of Colloid and Interface Science. 175*(1), 239–252. https://doi.org/10.1006/jcis.1995.1452
64. Pearl, S.H., Rand, M.J., Gantzer, P.A., Herndon, E.M., Geshnigani, M.A., Kjeldsen, T.R., Bryant, L.D. (2025) Manganese in drinking-water reservoirs: a multi-disciplinary review of current issues, biogeochemical controls, and oxygenation-based management. *Journal of Environmental Management*. *395*, 127573. https://doi.org/10.1016/j.jenvman.2025.127573
65. Phan Quang, H.H., Phan, K.T., Dinh, N.T., Tran Thi, T.N., Kajitvichyanukul, P., Raizada, P., Singh, P., Nguyen, V.-H. (2022) Using ZrO_2 coated sludge from drinking water treatment plant as a novel adsorbent for nitrate removal from contaminated water. *Environmental Research*. *212*, 113410. https://doi.org/10.1016/j.envres.2022.113410
66. Piccin, J.S., Dotto, G.L., Pinto, L. a. A. (2011) Adsorption isotherms and thermochemical data of FD&C Red n° 40 binding by Chitosan. *Brazilian Journal of Chemical Engineering*. *28*, 295–304. https://doi.org/https://doi.org/10.1590/S0104-66322011000200014
67. Pookmanee, P., Thippraphan, P., Phanichphant, S. (2011) Removal of heavy metals from aqueous solution by natural and modified diatomite. *Journal of the Microscopy Society of Thailand*. *4*(2), 103–107.
68. Rahman, Md.W., Ong, H.R., Kong, W.Y.J., Abdullah, H., Khan, Md.M.R. (2021) Adsorption of manganese ions from aqueous solution by using manganese oxide coated zeolite. *Desalination and Water Treatment*. 224, 273–281. https://doi.org/10.5004/dwt.2021.27174
69. Ramirez, K.G., Possan, E., Bittencourt, P.R.S., Carneiro, C., Colombo, M. (2018) Physico-chemical characterization of centrifuged sludge from the Tamanduá water treatment plant (Foz do Iguaçu, PR). *Matéria (Rio de Janeiro)*. *23*(3). https://doi.org/10.1590/s1517-707620180003.0521
70. Riad, M.H. (2025) From tradition to innovation: An in-depth review of manganese removal techniques in water treatment. *Environmental Research and Technology*. *8*(3), 741–754. https://doi.org/10.35208/ert.1538816
71. Ribeiro, P.L., Bamberg, A.L., Dos Santos Pereira, I., Monteiro, A.B., Da Luz Potes, M. & De Lima, C.L.R. (2022) Water treatment residuals for ameliorating sandy soils: Implications in environmental, soil and plant growth parameters. *Geoderma*. *407*, 115537. https://doi.org/10.1016/j.geoderma.2021.115537
72. Robati, D. (2013) Pseudo-second-order kinetic equations for modeling adsorption systems for removal of lead ions using multi-walled carbon nanotube. *Journal of Nanostructure in Chemistry*. *3*(1), 55. https://doi.org/10.1186/2193-8865-3-55
73. Rumsby, P., Rockett, L., Clegg, H., Jonsson, J., Benson, V., Harman, M., Doyle, T., Rushton, L., et al. (2014) Speciation of manganese in drinking water. *Toxicology Letters*. *229*, S120. https://doi.org/10.1016/j.toxlet.2014.06.431
74. Santiago Martins, D., Ramos Estevam, B., Larisson Toninatto Vilela, R., Deodato Isique, W., Freire Boina, R. (2022) Lodo de estação de tratamento de água como adsorvente: preparo e caracterização. *Revista DAE*. *71*(239), 6–16. https://doi.org/10.36659/dae.2023.001
75. Sharma, Y.C., Uma, Singh, S.N., Paras, Gode, F. (2007) Fly ash for the removal of Mn(II) from aqueous solutions and wastewaters. *Chemical Engineering Journal*. *132*(1–3), 319–323. https://doi.org/10.1016/j.cej.2007.01.018
76. Silva, J.R., de Carvalho, M.H., Dantas de Jesus, A.M., Fiore, F.A. (2025) Effect of thermal drying on the physico-chemical and microbiological characteristics of drinking water treatment sludge. *Cleaner Engineering and Technology*. *26*, 100947. https://doi.org/10.1016/j.clet.2025.100947
77. Siswoyo, E., Qoniah, I., Lestari, P., Fajri, J.A., Sani, R.A., Sari, D.G., Boving, T. (2019) Development of a floating adsorbent for cadmium derived from modified drinking water treatment plant sludge. *Environmental Technology & Innovation*. *14*, 100312. https://doi.org/10.1016/j.eti.2019.01.006
78. Sivalingam, S., Gopal, V. (2024) Low-cost adsorbent from biomass for removal of Fe(II) and Mn(II) for water treatment: batch and column adsorption study. *Chemical Papers. 78*(8), 4891–4908. https://doi.org/10.1007/s11696-024-03438-x
79. Skubiszewska-Zięba, J., Charmas, B., Leboda, R., Gun'ko, V.M. (2012) Carbon-mineral adsorbents with a diatomaceous earth/perlite matrix modified by carbon deposits. *Microporous and Mesoporous Materials*. *156*, 209–216. https://doi.org/10.1016/j.micromeso.2012.02.038
80. Sousa, D., Bernardo, M., Matos, I., Fonseca, I., Dias, R., Maurício, R. (2025) Key properties of drinking water treatment residuals for their effective reuse as phosphate adsorbents. *Environmental Processes*. *12*(3), 39. https://doi.org/10.1007/s40710-025-00780-4
81. Sousa, D., Bernardo, M., Sellaoui, L., Bonilla-Petriciolet, A., Mokhati, A., Maurício, R. (2025) Reuse of drinking water treatment sludge for the removal of antibiotics: The case study of sulfamethoxazole and trimethoprim based on advanced statistical physics models. *Journal of Hazardous Materials Advances*. *18*, 100737. https://doi.org/10.1016/j.hazadv.2025.100737

82. Stookey, L.L. (1970) Ferrozine - a new spectrophotometric reagent for iron. *Analytical Chemistry*. *42*(7), 779–781. https://doi.org/10.1021/ac60289a016
83. Tobiason, J.E., Bazilio, A., Goodwill, J., Mai, X., Nguyen, C. (2016) Manganese removal from drinking water sources. *Current Pollution Reports*. *2*(3), 168–177. https://doi.org/10.1007/s40726-016-0036-2
84. Tran, H.N., You, S.-J., Hosseini-Bandegharaei, A., Chao, H.-P. (2017) Mistakes and inconsistencies regarding adsorption of contaminants from aqueous solutions: A critical review. *Water Research*. *120*, 88–116. https://doi.org/10.1016/j.watres.2017.04.014
85. Tran, T.N., Kim, D.-G., Ko, S.-O. (2018) Adsorption mechanisms of manganese (II) ions onto acid-treated activated carbon. *KSCE Journal of Civil Engineering*. *22*(10), 3772–3782. https://doi.org/10.1007/s12205-018-1334-6
86. Truong, T.V., Tiwari, D., Mok, Y.S., Kim, D.-J. (2021) Recovery of aluminum from water treatment sludge for phosphorus removal by combined calcination and extraction. *Journal of Industrial and Engineering Chemistry*. *103*, 195–204. https://doi.org/10.1016/j.jiec.2021.07.033
87. Tseng, R.-L., Tseng, S.-K. (2005) Pore structure and adsorption performance of the KOH-activated carbons prepared from corncob. *Journal of Colloid and Interface Science*. *287*(2), 428–437. https://doi.org/10.1016/j.jcis.2005.02.033
88. Varatharajan, G.R., Ndayishimiye, J.C., Nyirabuhoro, P. (2025) Emerging contaminants: a rising threat to urban water and a barrier to achieving SDG-aligned planetary protection. *Water*. *17*(16), 2367. https://doi.org/10.3390/w17162367
89. Vitorette, P.J., Zaccaron, A., Müller, T.G., De Oliveira, C.M., Peterson, M., Raupp-Pereira, F. (2022) Analysis of solid waste discharged from water treatment plant as a fluoride-absorbing functional material. *Groundwater for Sustainable Development*. *17*, 100765. https://doi.org/10.1016/j.gsd.2022.100765
90. Wang, L., Li, M., Hao, M., Liu, G., Xu, S., Chen, J., Ren, X., Levendis, Y.A. (2021) Effects of activation conditions on the properties of sludge-based activated coke. *ACS Omega*. *6*(34), 22020–22032. https://doi.org/10.1021/acsomega.1c02600
91. Wu, C.-H., Lin, C.-F., Chen, W.-R. (2004) Regeneration and reuse of water treatment plant sludge: adsorbent for cations. *Journal of Environmental Science and Health, Part A*. *39*(3), 717–728. https://doi.org/10.1081/ESE-120027737
92. Yang, K., Sun, J., Liu, H., Yang, W., Dong, L. (2023) Study on the thermogravimetric kinetics of dehydrated sewage sludge regulated by cationic polyacrylamide and sawdust. *Polymers. 15*(10), 2396. https://doi.org/10.3390/polym15102396
93. Yavuz, Ö., Altunkaynak, Y., Güzel, F. (2003) Removal of copper, nickel, cobalt and manganese from aqueous solution by kaolinite. *Water Research*. *37*(4), 948–952. https://doi.org/10.1016/S0043-1354(02)00409-8
94. Zhang, F.-S., Itoh, H. (2003) Adsorbents made from waste ashes and post-consumer PET and their potential utilization in wastewater treatment. *Journal of Hazardous Materials*. *101*(3), 323–337. https://doi.org/10.1016/S0304-3894(03)00208-5
95. Zhang, Y., Yang, L., Wang, D., Zhang, T. (2015) Resource utilization of water treatment residual sludge (WTRS): effective defluoridation from aqueous solution. *Desalination and Water Treatment*. *55*(2), 448–462. https://doi.org/10.1080/19443994.2014.918904
96. Zhang, Y., Xu, X., Geng, Q., Li, Q., Li, X., Wang, Y., Tang, Z., Gao, B., et al. (2025) Redefining the roles of alkali activators for porous carbon. *Chemical Science*. *16*(4), 2034–2043. https://doi.org/10.1039/d4sc07145j
97. Zhao, W., Xie, H., Li, J., Zhang, L., Zhao, Y. (2021) Application of alum sludge in wastewater treatment processes: 'science' of reuse and reclamation pathways. *Processes*. *9*(4), 612. https://doi.org/10.3390/pr9040612